Quantum Interference in the Hyperfine Transitions of Ytterbium

Adam Dee Dodson

A senior thesis submitted to the faculty of
Brigham Young University
in partial fulfillment of the requirements for the degree of

Bachelor of Science

Scott Bergeson, Advisor

Department of Physics and Astronomy

Brigham Young University

ABSTRACT

Quantum Interference in the Hyperfine Transitions of Ytterbium

Adam Dee Dodson
Department of Physics and Astronomy, BYU
Bachelor of Science

Emission spectra from atoms with hyperfine structure typically show closely-spaced atomic transitions. This happens because the hyperfine interaction splits and shifts the fine-structure energy levels in both the ground and excited state by a small amount. In laser-induced fluorescence measurements, the atoms are driven into a superposition of excited hyperfine states which then decay into a range of ground hyperfine states. Interference in different quantum pathways for this process influences the probability of excitation. Unless this is properly accounted for, this interference effect systematically shifts the apparent center of the fluorescence lineshape. We report measurements of this quantum interference (QI) effect in Yb-171 and Yb-173 and show that QI shifts the line centers by up to 5 MHz. We extend and verify a published QI model for Yb-171. We show that optical pumping complicates a straightfoward application of the model to the experiment for Yb-173. We then demonstrate that optical pumping-induced variations in the distribution of magnetic sub-levels in the hyperfine structure are insufficient to explain observed shifts in Yb-173.

Keywords: hyperfine structure, quantum interference, laser-induced fluorescence, ytterbium, isotope shift, precision spectroscopy, laser metrology

ACKNOWLEDGMENTS

This research was supported by Brigham Young University and by grants from the National Science Foundation under Grant No. PHY-1500376 and from the Air Force Office of Scientific Research under Grant No. AFOSR-FA9550-17-1-0302.

Contents

List of Figures

List of Tables

Chapter 1

Introduction

1.1 Motivation

Correct measurements of atomic transitions are important for benchmarking atomic structure calculations as well as constraining the search for new physics beyond the standard model [1]. It is, therefore, important to have accurate data on the atomic transitions for a given atom. Recent research has revealed that fluorescence measurements of closely-spaced atomic transitions, specifically transitions to hyperfine levels, are subject to the effects of quantum interference (QI). Unfortunately, many past fluorescence measurements of hyperfine transitions have failed to account for this interference. This is problematic because the failure to account for QI can result in systematic errors of up to several MHz [2–4].

The main goal of our work is to verify the existing QI model for the odd isotopes of ytterbium (^{171}Yb and ^{173}Yb). In this thesis, I will present our work verifying the QI model for a single transition in ^{171}Yb ($F = 1/2 \rightarrow F' = 3/2$). In addition, I will present the difficulties of fully verifying the model in ^{173}Yb. My specific contributions to this project are assisting in data acquisition, developing the QI model for Yb which includes the effect of optical pumping in the hyperfine sub-levels, and

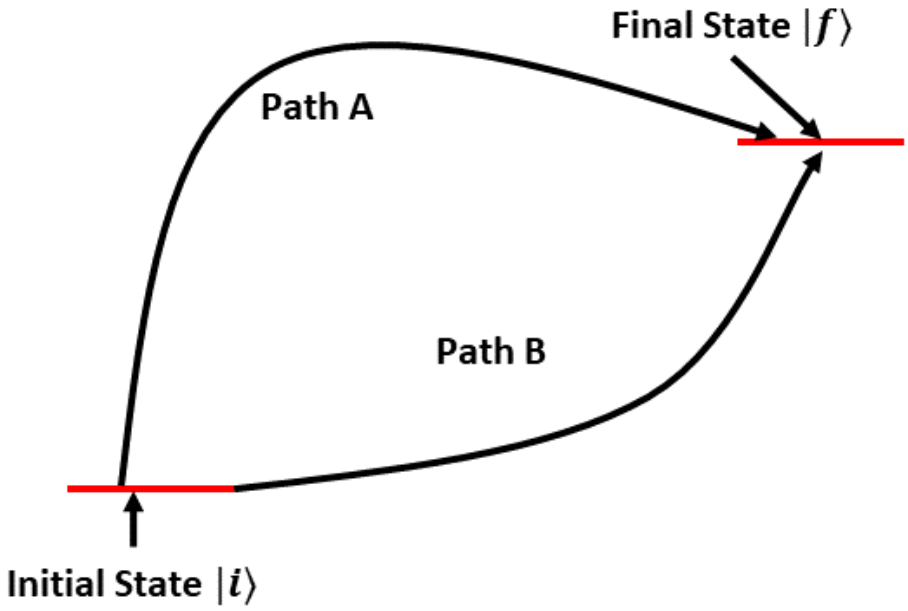

Figure 1.1 Generic quantum interference scenario featuring two interfering paths between the initial and final state. In quantum mechanics, paths A and B differ by a phase factor. The probability of a transition from $|i\rangle$ to $|f\rangle$ is modulated by this phase difference.

fitting the measured data to the model.

1.2 Quantum Interference

Quantum interference occurs when two or more possible quantum path are allowed. Figure 1.1 shows a generic scenario where quantum interference occurs. An initial state $|i\rangle$ and a final state $|f\rangle$ are connected by two possible pathways, path A and path B. If we took an arbitrary quantum system and moved it from $|i\rangle$ to $|f\rangle$, we would observe behavior that is not the sum of how paths A and B behave in isolation. The interaction between the paths forces the inclusion of an additional factor to characterize how the paths interfere with one another.

In quantum mechanics, a matrix element characterizes the quantum amplitude for a quantum system moving along a specific path. For the scenario in Figure 1.1, the matrix elements for paths A

and B are A_{fi} and B_{fi}. The probability, which tells us how the quantum system behaves when both pathways are available, is calculated as

$$P_{i\to f} = \left| A_{fi} + B_{fi} e^{i\phi} \right|^2, \tag{1.1}$$

where ϕ is the phase angle that characterizes the phase difference between the pathways. Assuming that the matrix elements are real, we write

$$P_{i\to f} = \left|A_{fi}\right|^2 + \left|B_{fi}\right|^2 + 2A_{fi}B_{fi}\cos(\phi). \tag{1.2}$$

This equation is fairly simple to understand. The first term: $\left|A_{fi}\right|^2$ is the transition probability when only path A is available. The second term, $\left|B_{fi}\right|^2$, is the transition probability when only path B is available. The final term: $2A_{fi}B_{fi}\cos(\phi)$ is the quantum interference term, showing how the transition probability is modulated when both paths are available. Notice that the result is the paths' behavior in isolation plus an additional factor to characterize how they interfere.

This illustrates the principle of QI. If there are multiple available pathways between some initial and final state, interference results. In a laser-induced fluorescence experiment, light interacts with an atom and is scattered. In the course of the interaction, the atom is moved between an initial and final state. In the absence of atomic hyperfine structure , there is only one available path between the states. However, for atoms with hyperfine structure, excitation occurs through a superposition of excited states, giving multiple paths through which fluorescence can occur. In a laser-induced fluorescence experiment, QI should affect the fluorescence lineshape. Scientists at NIST have published a careful analysis which modeled the fluorescence lineshape in lithium and showed that QI does indeed affect fluorescence lineshapes [4].

1.3 Ytterbium-173 and Ytterbium-171

We extended the NIST QI model to Yb. This atom has two stable isotopes with hyperfine structure ^{171}Yb and ^{173}Yb. Both of these isotopes have an easily accessible transition at 399 nm ($6s^2$

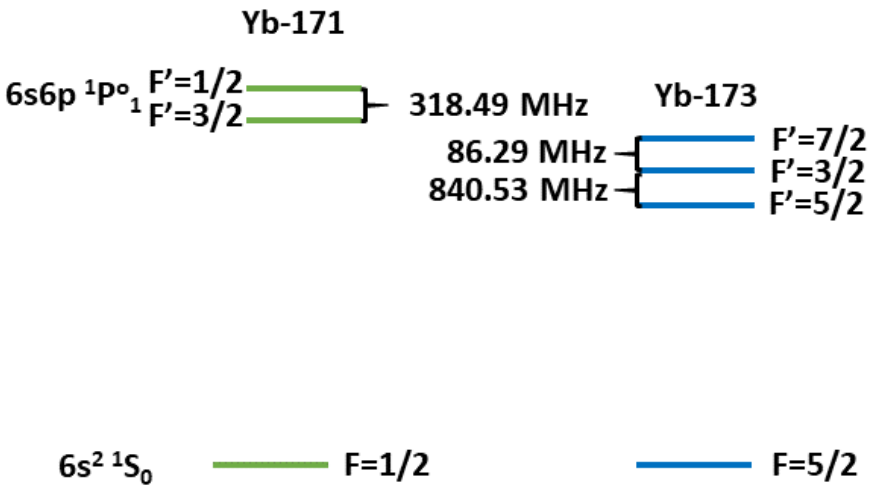

Figure 1.2 Hyperfine splitting in Yb-173 and Yb-171. The hyperfine splitting is caused by the interaction of the nuclear magnetic moment and the electronic spin-orbit magnetic moment. Because the ground state has $j = 0$, there is no hyperfine splitting in that state. The hyperfine splittings are taken from Refs. [1, 2]

$^1S_0 \rightarrow 6s6p\ ^1P_1^\circ$) where the excited state ($6s6p\ ^1P_1^\circ$) splits into multiple hyperfine levels. That means that we have a closely-spaced, accessible, atomic transition with which to test the QI model. Figure 1.2 shows the level structure of this transition for both isotopes including the splitting of the excited states.

1.4 Optical Pumping

Generically, optical pumping refers to using light to raise a medium or some of its constituents to higher energy levels [5]. In a laser-induced fluorescence spectroscopy experiment it also describes how interactions with a laser can place atoms into non-thermal distributions. Even though the $6s^2\ ^1S_0$ has no hyperfine structure (see Fig. 1.2), the $F = \frac{1}{2}$ and $F = \frac{5}{2}$ ground states have several magnetic sub-levels. In the absence of an external magnetic field these sub-levels have the same energy. When the atoms are in thermal equilibrium, these sub-levels are equally populated. However, when

ytterbium cycles through several S to P transitions, the population distribution in these sub-levels can change. The population distribution that the atoms achieve is determined by the decay coefficients of the excited state magnetic sub-levels.

1.5 Previous Work

The groundwork for the quantum interference of hyperfine transitions was laid by a Roger Brown, et al. [3]. In their work they noted that there were multiple discrepancies in the measured values for lithium transitions. These discrepancies, they said, might result from an incomplete lineshape model. After illustrating that the extracted line center from a Lorentzian fit depends on the polarization angle of the incident light, they sought to develop that more complete model of the atomic lineshape.

In a paper that followed soon after their initial observation, this same group showed that quantum interference between hyperfine transitions caused the angular dependence in the Lorentzian fits [4]. Beginning with Fermi's golden rule, they derived a more complete lineshape model. In their derivation, they noted that the quantum interference between hyperfine levels arose from a required summation and norm squared over all the possible excited states. That operation allows interference between the quantum amplitudes that describe the transition of an atom to the excited states. The result is an interference term whose strength depends on the energy spacing between the hyperfine levels. With the QI lineshape model established, they revisited the experimental data and showed that their model matched with great accuracy.

Our group has recently published work about ytterbium spectroscopy that mentioned the effect of quantum interference in the odd isotopes of ytterbium [1,2]. Our 2016 paper [2] published results for the isotope shifts of $6s^2\ {}^1S_0 \rightarrow 6s6p\ {}^1P_1^\circ$. In that paper, we noted the effect of QI in the F=1/2 to F'=3/2 transition found in ^{171}Yb. A more recent paper [1], published in January 2018, specifically highlighted the ^{173}Yb hyperfine splitting between the F'=3/2 and F'=7/2 and noted the presence of

quantum interference in both transitions. This thesis is a continuation of the QI work done in both papers.

1.6 Overview

In our next chapter, we will present our extension of the QI model to ^{173}Yb and ^{171}Yb. We will also present our optical pumping model and show how to account for non-thermal distributions of the ground level magnetic sub-levels. In Chapter 3, we will compare the predictions of the QI model to ^{171}Yb. We will then discuss the difficulties of applying that same model to ^{173}Yb.

Chapter 2

Modeling and Predictions

2.1 The Quantum Interference Model

In this section I present and discuss the QI lineshape model that was originally derived in Ref. [4]. The equation describing the QI lineshape is:

$$\frac{dR_{F_i}(\hat{\varepsilon}_L)}{d\Omega_s} = \frac{1}{4\pi}\frac{I}{I_0}\left(\frac{\Gamma}{2}\right)^3 \left\{ \sum_{F'} \frac{f(\mathbf{k}_s, \hat{\varepsilon}_L, F_i, F')}{(\Delta_{F_i}^{F'})^2 + (\Gamma/2)^2} + \sum_{F' \neq F''} 2Re\left[\frac{g(\mathbf{k}_s, \hat{\varepsilon}_L, F_i, F', F'')}{(\Delta_{F_i}^{F'} + i\Gamma/2)(\Delta_{F_i}^{F''} - i\Gamma/2)} \right] \right\} \quad (2.1)$$

where I is the laser intensity, I_0 is the saturation intensity of the transition and Γ is $1/\tau$ where τ is the excited state lifetime.

Since the equation is lengthy and complex, I will explain it piece by piece. The first summation over F' is called the Lorentzian term and it represents how an atom scatters near-resonant light in the absence of interference. The strength of this term depends on several factors. The first of these factors is called the laser detuning from the atomic resonance $\Delta_{F_i}^{F'}$. When the detuning is small, i.e. when the laser frequency is close to the atomic resonance, the atom scatters more light.

Another factor influencing the strength of the Lorentzian term is the line strength $f(\mathbf{k}_s, \hat{\varepsilon}_L, F_i, F')$. This factor depends upon the laser polarization angle ($\hat{\varepsilon}_L$), the scattered light direction ($\mathbf{k}_s$), the

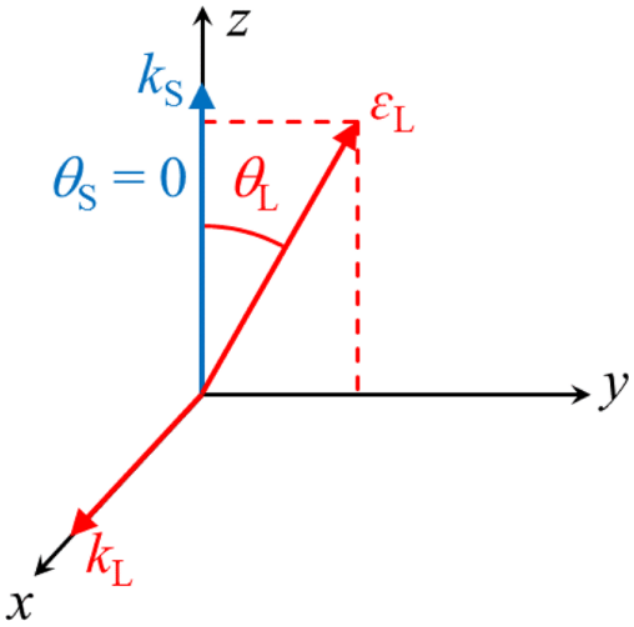

Figure 2.1 The coordinate system showing how θ_L and θ_s were determined in our experimental setup [2]

.

initial state (F_i) and the excited state (F'). After some simplication, the line strength is defined as:

$$f(\theta_s, \theta_L, F, F') = A_F^{F'} + \frac{B_F^{F'}}{2}(3\cos^2(\theta_s)\cos^2(\theta_L) - 1) \tag{2.2}$$

where θ_L is the laser polarization direction and θ_s is scatter light direction as told by Figure 2.1. The coefficients $A_F^{F'}$ and $B_F^{F'}$ for a specific transition can be calculated from the original work [3].

The second summation over F' is called the interference term. As with the Lorentzian term, the overall strength of the interference varies with the laser detuning Δ. However, the strength depends upon the detuning from two atomic resonances F' and F'', where F' and F'' are the interfering levels. This dependence allows the interfering term to be non-negligible only when both $\Delta_{F_i}^{F'}$ and $\Delta_{F_i}^{F''}$ are small simultaneously. Hence, the smaller the spacing between hyperfine levels, the stronger the resultant interference.

The numerator of the interference term is called the interference strength $g(\mathbf{k}_s, \hat{\varepsilon}_L, F_i, F', F'')$.

This term has the same dependencies as f with the added dependence on the interfering line F''. After the same simplifications that led to Eq. (2.2), the interference strength is defined as:

$$g(\theta_s, \theta_L, F, F', F'') = \frac{C_F^{F'}}{2}(3\cos^2(\theta_s)\cos^2(\theta_L) - 1). \tag{2.3}$$

Once again, the coefficient $C_F^{F'}$ can be calculated for a specific transition using the original work [4].

There is one more point that merits discussion: At a certain angle, referred to as the magic angle, the terms associated with $B_F^{F'}$ and $C_F^{F'}$ go to zero. At that angle, the QI term drops out and we are left with only the Lorentzian term for closely spaced lines. In our experimental configuration, $\theta_s = 0°$. This means that the magic angle occurs at $\arccos(\sqrt{1/3}) = 54.74°$. As will be shown later, when data taken at this angle is fit to a Lorentzian lineshape, the fit extracts the actual line center of the transition.

2.2 Optical Pumping Model

The model presented in the previous section implicitly assumes that the ground state magnetic sub-levels are thermally distributed. In their experimental work, the group at NIST was able to use low enough laser intensity to keep that assumption true. Our detectors, however, are not be able to detect signals that weak. As a result, we were forced to use a laser intensity that can induce shifts in the ground state magnetic sub-levels via optical pumping. Therefore, in order to apply the QI model, we need to predict how optical pumping perturbs the ground state magnetic sub-levels. Furthermore, we need to make a small correction to the definitions of f and g to account for this perturbation. Note that the model presented here assumes that the light is linearly polarized in order to be consistent with our experimental conditions.

First, I will present our model for optical pumping. To understand how this model will work, I will apply it to a simple scenario. Figure (2.2) shows this scenario. We have two levels of equal

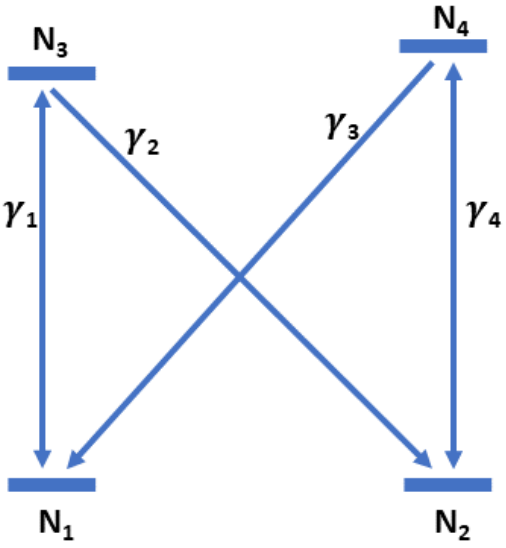

Figure 2.2 Here we have a scenario that shows a level structure with two ground and excited states. The transition probability γ_i for each path is noted. Equation 2.4 tells how the population of each level would change in time in the presence of a pumping laser.

energy in the ground state and two levels of near equal energy in the excited state. A laser of intensity I excites the atoms from the ground states to the excited states where they then decay back down to the ground states. With that picture in mind, the following set of coupled differential equations describes how the population in each state changes with time:

$$\begin{aligned}
\frac{dN_1}{dt} &= \frac{1}{\tau}\left(\gamma_1 N_3 + \gamma_3 N_4 - \frac{\gamma_1}{2}\frac{I}{I_0}(N_1 - N_3))\right) \\
\frac{dN_2}{dt} &= \frac{1}{\tau}\left(\gamma_2 N_3 + \gamma_4 N_4 - \frac{\gamma_4}{2}\frac{I}{I_0}(N_2 - N_4)\right) \\
\frac{dN_3}{dt} &= \frac{1}{\tau}\left(\frac{\gamma_1}{2}\frac{I}{I_0}(N_1 - N_3) - (\gamma_1 + \gamma_2)N_3\right) \\
\frac{dN_4}{dt} &= \frac{1}{\tau}\left(\frac{\gamma_4}{2}\frac{I}{I_0}(N_2 - N_4) - (\gamma_3 + \gamma_4)N_4\right)
\end{aligned} \tag{2.4}$$

where τ is the excited state lifetime, N_i is the population fraction of the ith level, γ_i is the appropriate Clebsch-Gordan coefficient, I is the laser intensity and I_0 is the saturation intensity of the transition.

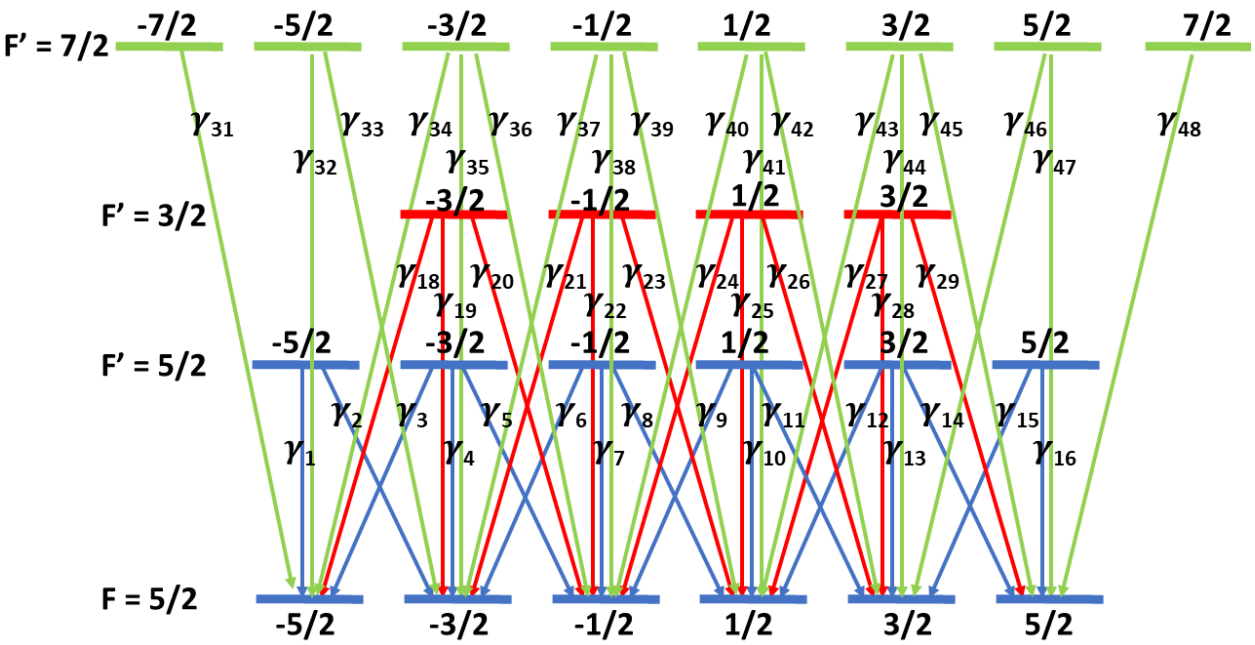

Figure 2.3 ^{173}Yb magnetic sub-level structure. The specific values of m_F are shown next to each level. To the left, the total atomic angular momentum, F, is shown. The connections between the individual states are labeled with a γ_i. The values for each γ_i can be found in Appendix B.

If we use matlab's ode45 solver, we can generate a numerical solution for the population fractions N_i as a function of time. The principles of this rate model will be applied to the more complex level structures of ^{171}Yb (Figure 2.3) and ^{173}Yb (Figure 2.4) in Chapter 3.

A small change to Eq. (2.2) and Eq. (2.3) is now in order. In the original derivation, before the simplifications that lead to Eq. (2.2) and Eq. (2.3), a factor of $1/g_T$ was included to account for the number of ground state magnetic sub-levels. Note that $g_T = \sum_i (2F_i + 1)$ [4]. This factor makes the assumption that the ground state magnetic sub-levels are thermally populated. If we remove $1/g_T$ and replace it with $P(m_i)$, the probability of being in a given Zeeman level, then the model can handle non-thermal populations. With that change, the equations now read:

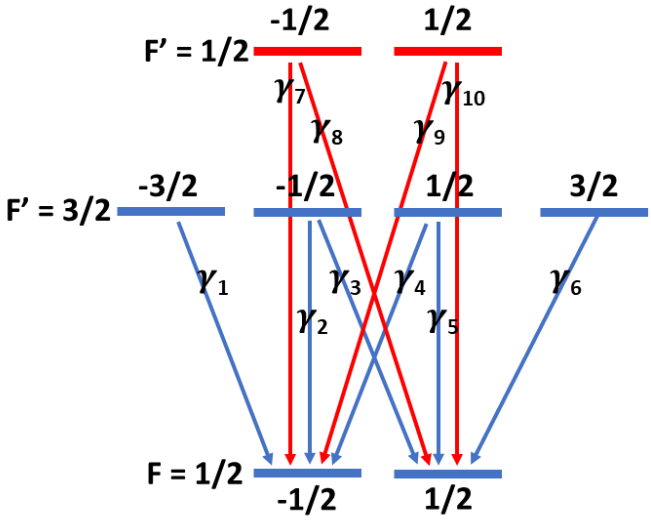

Figure 2.4 ^{171}Yb magnetic sub-level structure. The specific values of m_F are shown next to each level. To the left, the total atomic angular momentum, F, is shown. The connections between the individual states are labeled with a γ_i. The values for each γ_i can be found in Appendix B.

$$f\left(\mathbf{k}_s,\hat{\varepsilon},F_i,F'\right)=\frac{3}{2}\sum_{s,m_i,F_f,m_f}P(m_i)\left|C^{F'}_{i\to f}\left(\hat{\varepsilon}_s,\hat{\varepsilon}_L\right)\right|^2, \tag{2.5}$$

and

$$g\left(\mathbf{k}_s,\hat{\varepsilon},F_i,F',F''\right)=\frac{3}{2}\sum_{s,m_i,F_f,m_f}P(m_i)C^{F'}_{i\to f}\left(\hat{\varepsilon}_s,\hat{\varepsilon}_L\right)\left[C^{F''}_{i\to f}\left(\hat{\varepsilon}_s,\hat{\varepsilon}_L\right)\right]^*. \tag{2.6}$$

Note that these can be simplified down to the form of Eq. (2.2) and Eq. (2.3) to obtain the A, B and C coefficients. This format, however, is more convenient for showing the change. These modified equations will enable us to account for any variations in the magnetic sub-levels, including frequency dependent variations that end up arising in ^{173}Yb. We are now in a position to apply the QI and optical pumping models to ^{171}Yb and ^{173}Yb.

Chapter 3

Predictions and Comparisons

3.1 Comparison of data and model for ^{171}Yb

3.1.1 Optical Pumping

Shifts in the ground state magnetic sub-levels due to optical pumping do not occur in ^{171}Yb because the decay coefficients of the excited state magnetic sub-levels are symmetric. We used Tables B.4 and B.5 in tandem with Figure 2.4 to generate the appropriate system of equations to confirm that no shifts occur (see Appendix A). Based on our simulation, we can apply the QI model to ^{171}Yb without needing to account for optical pumping.

3.1.2 Quantum Interference Model

Using the methods described in Ref. [4], we generated the appropriate A, B and C coefficients for the F'=1/2 and F'=3/2 lines (See Table 3.1). Those coefficients allowed us to use Eq. (2.1) to generate lineshapes that we could then compare to the data. Unfortunately, we only have data on the F'=3/2 line since the F'=1/2 line is blended with the resonance peak of another isotope (^{170}Yb) making clean data difficult to obtain. In order to show the validity of the QI model for the F'=3/2

Table 3.1 Calculated A, B and C coefficients for the ^{171}Yb $6s^2\ ^1S_0 \rightarrow 6s6p\ ^1P_1^\circ$ transition.

F	F'	$A_F^{F'}$	$B_F^{F'}$	$C_F^{F'F''}$
1/2	3/2	8/9	-4/9	-4/9
1/2	1/2	4/9	0	-4/9

transition, I will present the results of the fit of the F'=3/2 transition data to a Lorentzian lineshape and the full QI lineshape. This will also make clear the systematic error introduced by assuming a purely Lorentzian lineshape.

When we perform the fits of the data, we extract the apparent location of the transition line center. We can then take the extracted line centers from both fitting routines and calculate their shift from the published line center frequency [2]. Figure 3.1 shows those shifts from the published line center frequency as a function of angle. The extracted line centers from the fit to the full QI lineshape (black) match the published line center frequency with minimal deviation and suggest that the QI model is valid. Contrast this with the angular dependence seen in the extracted line centers from the Lorentzian fit (blue). As expected, there is a systematic shift in the extracted line centers of the Lorentzian fit that disappears at the magic angle (54°).

As an additional verification of the QI model, we generated the full QI lineshape from the QI model and then fit it to a Lorentzian lineshape. Figure 3.1 shows the extracted line centers from that fit (red). If the model is correct, one would expect the blue and red data points to map out the same line. Based on Figure 3.1, they do indeed map out the same line with a small exception that can be attributed to a systematic error described in the figure caption. From Figure 3.1 we can conclude that QI does alter how ^{171}Yb scatters near-resonant photons and that the model we adapted from Ref. [4] accurately describes the data.

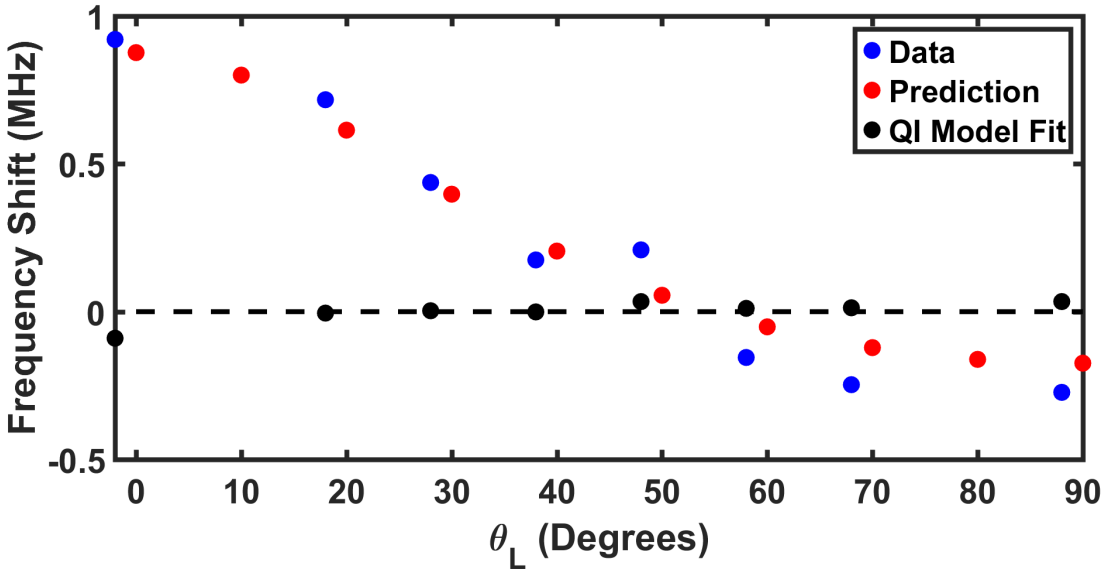

Figure 3.1
Here the extracted line centers of a Lorentzian fit to the data (blue) and the prediction (red) are shown. The extracted line centers for the full QI fit of the data are also show (black). The x-axis is the laser polarization θ_L which is determined from Fig. 2.1. The y-axis is the shift from the true line center of the F'=3/2 transition. All the fittings were done by allowing the line center, line width and signal offset to be fit parameters. One can see that the agreement between the extracted Lorentzian line centers of the data (blue) and the prediction (red) is quite good until $\approx 60°$. This discrepancy is a systematic error caused by fitting non-Lorentzian data to a Lorentzian lineshape. As noted in the text, the Lorentzian lineshape fitting of the data (blue) extracts the true line center at $\theta_L \approx 54°$.

3.2 Comparison of data and model for ^{173}Yb

3.2.1 Optical Pumping

In all of the transitions we are considering for ^{173}Yb (F'=3/2,5/2 and 7/2), optical pumping will force the atoms into non-thermal distributions of the magnetic sub-levels. At the laser intensity that we used in the laser-induced fluoresence experiment ($I \approx 10$ mW/cm^2), the optical pumping model (see Appendix A) shows that the atoms reach equilibrium with the laser in less than 0.5 microseconds. Since the atoms interact with the laser for ≈10 microseconds, we can safely assume that the majority of the scattered light signal comes from atoms whose magnetic sub-levels are in equilibrium with the laser.

Unfortunately, the magnetic sub-level distribution changes with laser frequency, making a direct comparison of the data with model problematic. Based on the coefficients given in Tables B.1 to B.3, the atoms will reach a different distribution of magnetic sub-levels depending upon which transition is being excited. If the transitions are reasonably separated, we can assume that in the neighborhood of the transition, the distribution it generates dominates. For the F'=5/2 transition this is true, but significant background from nearby transitions of other isotopes makes high quality data of this transition difficult to obtain. Unfortunately, the remaining transitions, F'=3/2 and F'=7/2, are separated by only $\Delta_{7/2}^{3/2} = 86.29$ MHz [1]. As a result, the equilibrium distribution of magnetic sub-levels changes with the laser detuning. Figure 3.2 shows the equilibrium ground state magnetic sub-levels for ^{173}Yb as a function of laser detuning from the F'=3/2 transition. If the QI strength depends upon the ground state magnetic sub-level distribution, and it does, then the QI strength changes as one scans a laser across the transition.

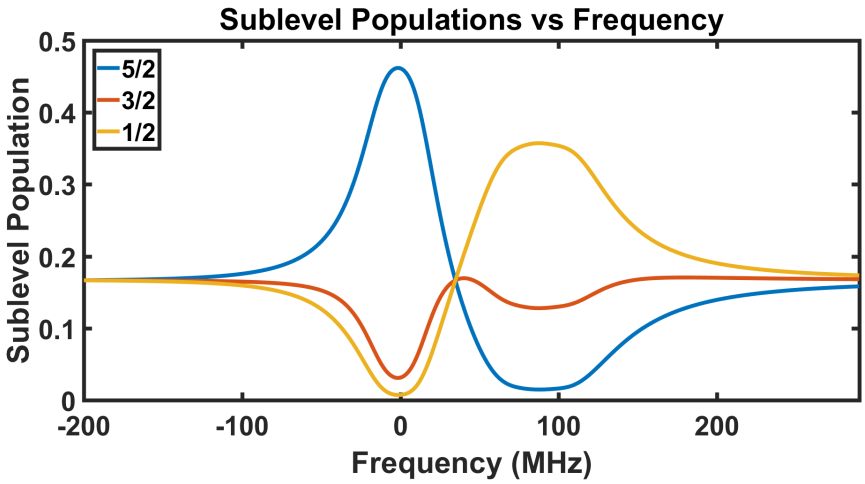

Figure 3.2 Variation in the ground state magnetic sub-levels as a function of detuning from the F'=3/2 transition. Note that only the positive m_F level populations are shown because their corresponding negative m_F level populations are identical. Notice also how the population fractions drastically as one scans a laser across the F'=3/2 and F'=7/2 transitions.

3.2.2 Quantum Interference Model

The magnetic sub-level variations introduced by optical pumping alter the QI strength and preclude a straightforward application of the QI model. This is clear in Figure 3.3 which shows both the line (f) and interference (g) strengths for the F'=7/2 and F'=3/2 lines as a function of detuning from the F'=3/2 line. Regardless of optical pumping difficulties, we can still compare the features of the data to the predictions of the model.

Using our experimental conditions, we generated the magnetic sublevel populations and the resultant lineshape for F'=7/2 and F'=3/2 lines. We then fit the predicted lineshape to a sum of two Lorentzians and extracted the line centers of those fits. Figure 3.4 shows those extracted line centers. We then took the actual data and performed the same fit. The extracted line centers for the F'=7/2 and F'=3/2 data are shown in Figures 3.5 and 3.6 respectively. It is clear, unfortunately, the predicted amplitude of the systematic shifts are inconsistent with the data. The direction of the shift matches but the amplitude is smaller by a factor of roughly two. It is unclear as to the cause of this

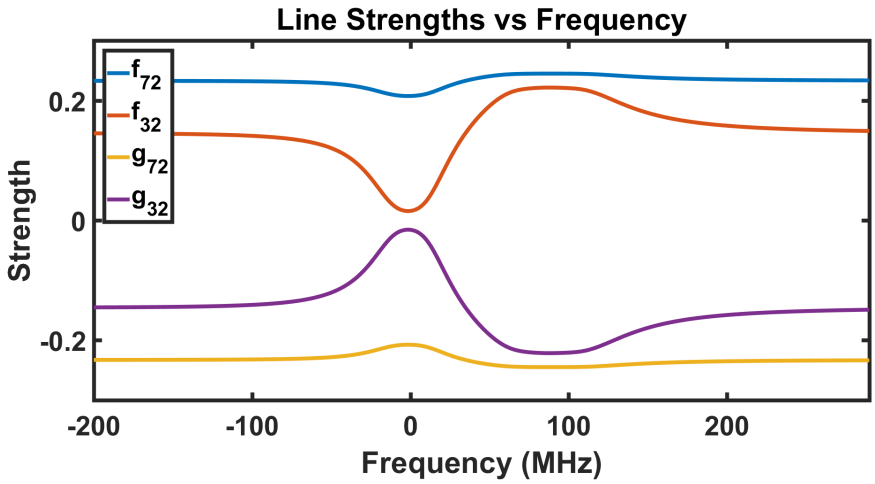

Figure 3.3 Line and Interference Strengths for the F'=3/2 and F'=7/2 as a function of detuning from the F'=3/2 line. In the region of the F'=3/2 transition, the strengths vary significantly.

difference.

Initially, we looked to determine if the optical pumping model was in error. We noticed that the amplitude of the systematic shift increased as the atoms were driven the $m_F = \pm 1/2$ state. Since the experimental conditions drive the atoms that direction, we reasoned that perhaps the optical pumping model was underestimating that shift. Along those lines, we assumed that only $m_F \pm 1/2$ was populated and generated the resultant lineshape. We then performed the same Lorentzian fit described above, we found that the expected systematic shifts in the line center were still to small to explain the experimental result.

In our final attempt to reconcile the data and the model, we did a direct comparison of the model to the data rather than simply comparing the systematic shifts. We generated the expected lineshapes for each angle and then overlaid the data on the generated lineshapes and compared them. In this direct comparison, we noted that the relative amplitudes of the F'=3/2 and F'=7/2 lines in the model also differ from the relative amplitudes in the data. Once again, we do not know why that difference occurs.

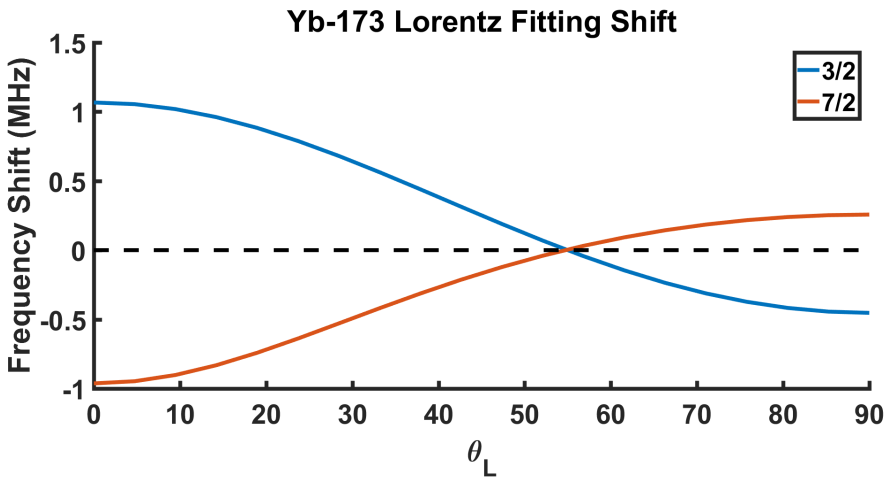

Figure 3.4 Frequency shifts of the extracted line centers from a two Lorentzian fit of the F'=7/2 and F'=3/2 prediction. The fits were conducted by allowing the peak locations and their amplitudes to be fit parameters.

Based on our analysis, we conclude that there is an additional effect that we are failing to account for that is altering the lineshape. One candidate for this effect is the presence of the pumping laser tuned to F'=5/2. It may be that this laser is somehow altering how the atoms transition and thus altering the lineshape. Further study is needed to determine what the actual effect is and how to model is appropriately.

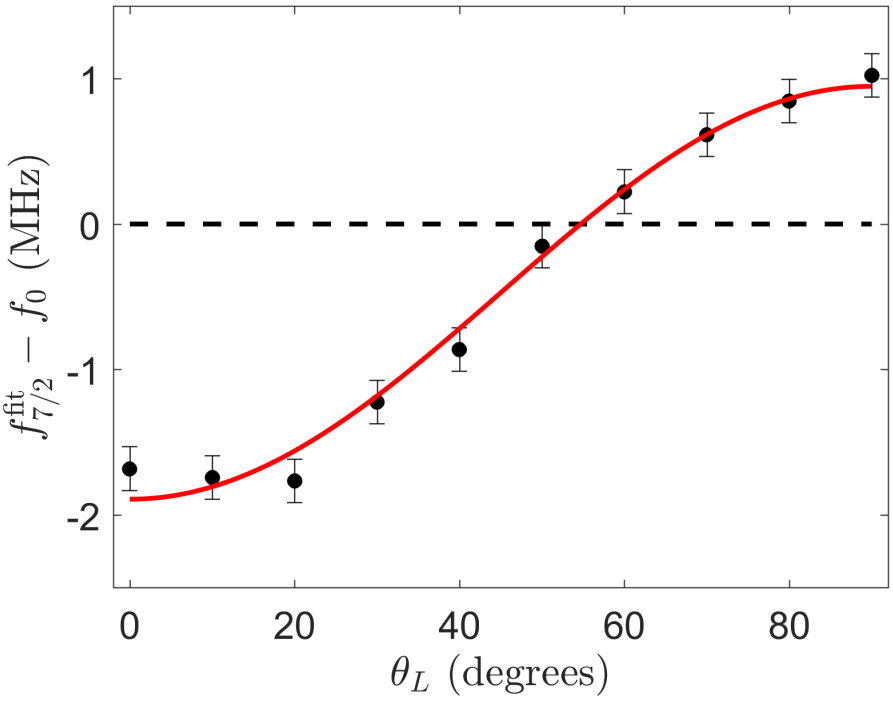

Figure 3.5 Extracted line centers for the F'=7/2 line from a two Lorentzian fit of the ^{173}Yb F'=7/2 and F'=3/2 data. The fit parameters were the peak locations, peak widths and peak amplitudes. Notice how the fit to the data reproduces the shift direction seen in Fig. 3.4. Taken from [2]

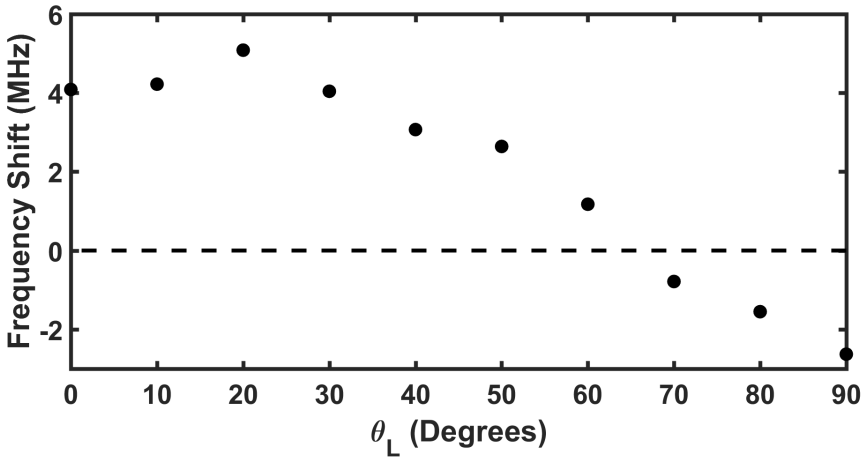

Figure 3.6 Extracted line centers for the F'=3/2 line from a two Lorentzian fit of the ^{173}Yb F'=7/2 and F'=3/2 data. The fitting techniques were identical to that of 3.5. Notice that the fit to the data also reproduces the shift direction seen in Fig. 3.4

Appendix A

Optical Pumping Coupled Equations

The coupled equations we used for calculating the optical pumping in ^{173}Yb is:

$$\frac{dN_1}{dt} = \frac{1}{\tau}\left(-\frac{I_{52}}{2I_0}\gamma_1(N_1-N_7) - \frac{I_{72}}{2I_0}\gamma_{32}(N_1-N_{18})\right.$$
$$\left.+\gamma_1 N_7 + \gamma_3 N_8 + \gamma_{18} N_{13} + \gamma_{31} N_{17} + \gamma_{32} N_{18} + \gamma_{34} N_{19}\right) \quad \text{(A.1)}$$

$$\frac{dN_2}{dt} = \frac{1}{\tau}\left(-\frac{I_{52}}{2I_0}\gamma_4(N_2-N_8) - \frac{I_{72}}{2I_0}\gamma_{35}(N_2-N_{19}) - \frac{I_{32}}{2I_0}\gamma_{19}(N_2-N_{13})\right.$$
$$\left.+\gamma_2 N_7 + \gamma_4 N_8 + \gamma_6 N_9 + \gamma_{19} N_{13} + \gamma_{21} N_{14} + \gamma_{33} N_{18} + \gamma_{35} N_{19} + \gamma_{37} N_{20}\right) \quad \text{(A.2)}$$

$$\frac{dN_3}{dt} = \frac{1}{\tau}\left(-\frac{I_{52}}{2I_0}\gamma_7(N_3-N_9) - \frac{I_{72}}{2I_0}\gamma_{38}(N_3-N_{20}) - \frac{I_{32}}{2I_0}\gamma_{22}(N_3-N_{14})\right.$$
$$\left.+\gamma_5 N_8 + \gamma_7 N_9 + \gamma_9 N_{10} + \gamma_{20} N_{13} + \gamma_{22} N_{14} + \gamma_{24} N_{15} + \gamma_{36} N_{19} + \gamma_{38} N_{20} + \gamma_{40} N_{21}\right) \quad \text{(A.3)}$$

$$\frac{dN_4}{dt} = \frac{1}{\tau}\left(-\frac{I_{52}}{2I_0}\gamma_{10}(N_4-N_{10}) - \frac{I_{72}}{2I_0}\gamma_{41}(N_4-N_{21}) - \frac{I_{32}}{2I_0}\gamma_{25}(N_4-N_{15})\right.$$
$$\left.+\gamma_8 N_9 + \gamma_{10} N_{10} + \gamma_{12} N_{11} + \gamma_{23} N_{14} + \gamma_{25} N_{15} + \gamma_{27} N_{16} + \gamma_{39} N_{20} + \gamma_{41} N_{21} + \gamma_{43} N_{22}\right) \quad \text{(A.4)}$$

$$\frac{dN_5}{dt} = \frac{1}{\tau}\left(-\frac{I_{52}}{2I_0}\gamma_{13}(N_5-N_{11}) - \frac{I_{72}}{2I_0}\gamma_{44}(N_5-N_{22}) - \frac{I_{32}}{2I_0}\gamma_{28}(N_5-N_{16})\right.$$
$$\left.+\gamma_{11} N_{10} + \gamma_{13} N_{11} + \gamma_{15} N_{12} + \gamma_{26} N_{15} + \gamma_{28} N_{16} + \gamma_{42} N_{21} + \gamma_{44} N_{22} + \gamma_{46} N_{23}\right) \quad \text{(A.5)}$$

$$\frac{dN_6}{dt} = \frac{1}{\tau}\left(-\frac{I_{52}}{2I_0}\gamma_{16}(N_6-N_{12}) - \frac{I_{72}}{2I_0}\gamma_{47}(N_6-N_{23})\right.$$
$$\left.+\gamma_{14} N_{11} + \gamma_{16} N_{12} + \gamma_{29} N_{16} + \gamma_{45} N_{22} + \gamma_{47} N_{23} + \gamma_{48} N_{24}\right) \quad \text{(A.6)}$$

$$\frac{dN_7}{dt} = \frac{1}{\tau}\left(\frac{I_{52}}{2I_0}\gamma_1(N_1-N_7) - (\gamma_1+\gamma_2)N_7\right) \quad \text{(A.7)}$$

$$\frac{dN_8}{dt} = \frac{1}{\tau}\left(\frac{I_{52}}{2I_0}\gamma_4(N_2-N_8) - (\gamma_3+\gamma_4+\gamma_5)N_8\right) \quad \text{(A.8)}$$

$$\frac{dN_9}{dt} = \frac{1}{\tau}\left(\frac{I_{52}}{2I_0}\gamma_7(N_3-N_9) - (\gamma_6+\gamma_7+\gamma_8)N_9\right) \quad \text{(A.9)}$$

$$\frac{dN_{10}}{dt} = \frac{1}{\tau}\left(\frac{I_{52}}{2I_0}\gamma_{10}(N_4-N_{10}) - (\gamma_9+\gamma_{10}+\gamma_{11})N_{10}\right) \quad \text{(A.10)}$$

$$\frac{dN_{11}}{dt} = \frac{1}{\tau}\left(\frac{I_{52}}{2I_0}\gamma_{13}(N_5-N_{11}) - (\gamma_{12}+\gamma_{13}+\gamma_{14})N_{11}\right) \quad \text{(A.11)}$$

$$\frac{dN_{12}}{dt} = \frac{1}{\tau}\left(\frac{I_{52}}{2I_0}\gamma_{16}(N_6-N_{12}) - (\gamma_{15}+\gamma_{16})N_{12}\right) \quad \text{(A.12)}$$

$$\frac{dN_{13}}{dt} = \frac{1}{\tau}\left(\frac{I_{32}}{2I_0}\gamma_{19}(N_2-N_{13}) - (\gamma_{18}+\gamma_{19}+\gamma_{20})N_{13}\right) \quad \text{(A.13)}$$

$$\frac{dN_{14}}{dt} = \frac{1}{\tau}\left(\frac{I_{32}}{2I_0}\gamma_{22}(N_3 - N_{14}) - (\gamma_{21} + \gamma_{22} + \gamma_{23})N_{14}\right) \tag{A.14}$$

$$\frac{dN_{15}}{dt} = \frac{1}{\tau}\left(\frac{I_{32}}{2I_0}\gamma_{25}(N_4 - N_{15}) - (\gamma_{24} + \gamma_{25} + \gamma_{26})N_{15}\right) \tag{A.15}$$

$$\frac{dN_{16}}{dt} = \frac{1}{\tau}\left(\frac{I_{32}}{2I_0}\gamma_{28}(N_5 - N_{16}) - (\gamma_{27} + \gamma_{28} + \gamma_{29})N_{16}\right) \tag{A.16}$$

$$\frac{dN_{17}}{dt} = \frac{-\gamma_{31}N_{17}}{\tau} \tag{A.17}$$

$$\frac{dN_{18}}{dt} = \frac{1}{\tau}\left(\frac{I_{72}}{2I_0}\gamma_{32}(N_1 - N_{18}) - (\gamma_{32} + \gamma_{33})N_{18}\right) \tag{A.18}$$

$$\frac{dN_{19}}{dt} = \frac{1}{\tau}\left(\frac{I_{72}}{2I_0}\gamma_{35}(N_2 - N_{19}) - (\gamma_{34} + \gamma_{35} + \gamma_{36})N_{19}\right) \tag{A.19}$$

$$\frac{dN_{20}}{dt} = \frac{1}{\tau}\left(\frac{I_{72}}{2I_0}\gamma_{38}(N_3 - N_{20}) - (\gamma_{37} + \gamma_{38} + \gamma_{39})N_{20}\right) \tag{A.20}$$

$$\frac{dN_{21}}{dt} = \frac{1}{\tau}\left(\frac{I_{72}}{2I_0}\gamma_{41}(N_4 - N_{21}) - (\gamma_{40} + \gamma_{41} + \gamma_{42})N_{21}\right) \tag{A.21}$$

$$\frac{dN_{22}}{dt} = \frac{1}{\tau}\left(\frac{I_{72}}{2I_0}\gamma_{44}(N_5 - N_{22}) - (\gamma_{43} + \gamma_{44} + \gamma_{45})N_{22}\right) \tag{A.22}$$

$$\frac{dN_{23}}{dt} = \frac{1}{\tau}\left(\frac{I_{72}}{2I_0}\gamma_{47}(N_6 - N_{23}) - (\gamma_{46} + \gamma_{47})N_{23}\right) \tag{A.23}$$

$$\frac{dN_{24}}{dt} = \frac{-\gamma_{48}N_{24}}{\tau} \tag{A.24}$$

The coupled system of equations that we used for ^{171}Yb is:

$$\frac{dN_1}{dt} = \frac{1}{\tau}\left(-\frac{I_{32}}{2I_0}\gamma_2(N_1 - N_4) - \frac{I_{12}}{2I_0}\gamma_7(N_1 - N_7) + \gamma_1 N_3 + \gamma_2 N_4 + \gamma_4 N_5 + \gamma_7 N_7 + \gamma_9 N_8\right) \tag{A.25}$$

$$\frac{dN_2}{dt} = \frac{1}{\tau}\left(-\frac{I_{32}}{2I_0}\gamma_5(N_2 - N_5) - \frac{I_{12}}{2I_0}\gamma_{10}(N_2 - N_8) + \gamma_3 N_4 + \gamma_5 N_5 + \gamma_6 N_6 + \gamma_8 N_7 + \gamma_{10} N_8\right) \tag{A.26}$$

$$\frac{dN_3}{dt} = \frac{-\gamma_1 N_3}{\tau} \tag{A.27}$$

$$\frac{dN_4}{dt} = \frac{1}{\tau}\left(\frac{I_{32}}{2I_0}\gamma_2(N_1 - N_4) - \gamma_2 N_4 - \gamma_3 N_4\right) \tag{A.28}$$

$$\frac{dN_5}{dt} = \frac{1}{\tau}\left(\frac{I_{32}}{2I_0}\gamma_5(N_2 - N_5) - \gamma_4 N_5 - \gamma_5 N_5\right) \tag{A.29}$$

$$\frac{dN_6}{dt} = \frac{-\gamma_6 N_6}{\tau} \tag{A.30}$$

$$\frac{dN_7}{dt} = \frac{1}{\tau}\left(\frac{I_{12}}{2I_0}\gamma_7(N_1 - N_7) - \gamma_7 N_7 - \gamma_8 N_7\right) \tag{A.31}$$

$$\frac{dN_8}{dt} = \frac{1}{\tau}\left(\frac{I_{12}}{2I_0}\gamma_{10}(N_2 - N_8) - \gamma_9 N_8 - \gamma_{10} N_8\right) \tag{A.32}$$

Appendix B

Rate Coefficient Tables

Each of the following tables has six columns. In order they are: m_i, m_f, N_i, N_f, C-G and γ_i. The first two columns correspond to the initial and final magnetic sub-levels. The next two reference these magnetic sublevels to the coupled system of equations found in Appendix A. When referencing them to the system of equations, make sure to select the one corresponding to the correct isotope. The fifth column gives the Clebsch-Gordan coefficient corresponding to the transition between the excited state and ground state magnetic sub-levels. The final column references the fifth column to the respective γ_i for the coupled system in Appendix A.

Table B.1 Rate coefficients for transition between F'=3/2 and F=5/2 in ^{173}Yb. C-G stands for Clebsch-Gordan Coefficient.

m_i	m_f	N_i	N_f	C-G	γ_i
$-3/2$	$-5/2$	N_{13}	N_1	2/3	γ_{18}
$-3/2$	$-3/2$	N_{13}	N_2	4/15	γ_{19}
$-3/2$	$-1/2$	N_{13}	N_3	1/15	γ_{20}
$-1/2$	$-3/2$	N_{14}	N_2	2/5	γ_{21}
$-1/2$	$-1/2$	N_{14}	N_3	2/5	γ_{22}
$-1/2$	$1/2$	N_{14}	N_4	1/5	γ_{23}
$1/2$	$-1/2$	N_{15}	N_3	1/5	γ_{24}
$1/2$	$1/2$	N_{15}	N_4	2/5	γ_{25}
$1/2$	$3/2$	N_{15}	N_5	2/5	γ_{26}
$3/2$	$1/2$	N_{16}	N_4	1/15	γ_{27}
$3/2$	$3/2$	N_{16}	N_5	4/15	γ_{28}
$3/2$	$5/2$	N_{16}	N_6	2/3	γ_{29}

Table B.2 Rate coefficients for transition between F'=5/2 and F=5/2 in ^{173}Yb. C-G stands for Clebsch-Gordan Coefficient.

m_i	m_f	N_i	N_f	C-G	γ_i
$-5/2$	$-5/2$	N_7	N_1	5/7	γ_1
$-5/2$	$-3/2$	N_7	N_2	2/7	γ_2
$-3/2$	$-5/2$	N_8	N_1	2/7	γ_3
$-3/2$	$-3/2$	N_8	N_2	9/35	γ_4
$-3/2$	$-1/2$	N_8	N_3	16/35	γ_5
$-1/2$	$-3/2$	N_9	N_2	16/35	γ_6
$-1/2$	$-1/2$	N_9	N_3	1/35	γ_7
$-1/2$	$1/2$	N_9	N_4	18/35	γ_8
$1/2$	$-1/2$	N_{10}	N_3	18/35	γ_9
$1/2$	$1/2$	N_{10}	N_4	1/35	γ_{10}
$1/2$	$3/2$	N_{10}	N_5	16/35	γ_{11}
$3/2$	$1/2$	N_{11}	N_4	16/35	γ_{12}
$3/2$	$3/2$	N_{11}	N_5	9/35	γ_{13}
$3/2$	$5/2$	N_{11}	N_6	2/7	γ_{14}
$5/2$	$3/2$	N_{12}	N_5	2/7	γ_{15}
$5/2$	$5/2$	N_{12}	N_6	5/7	γ_{16}

Table B.3 Rate coefficients for transition between F'=7/2 and F'=5/2 in ^{173}Yb. C-G stands for Clebsch-Gordan Coefficient.

m_i	m_f	N_i	N_f	C-G	γ_i
$-7/2$	$-5/2$	N_{17}	N_1	1	γ_{31}
$-5/2$	$-5/2$	N_{18}	N_1	2/7	γ_{32}
$-5/2$	$-3/2$	N_{18}	N_2	5/7	γ_{33}
$-3/2$	$-5/2$	N_{19}	N_1	1/21	γ_{34}
$-3/2$	$-3/2$	N_{19}	N_2	10/21	γ_{35}
$-3/2$	$-1/2$	N_{19}	N_3	10/21	γ_{36}
$-1/2$	$-3/2$	N_{20}	N_2	1/7	γ_{37}
$-1/2$	$-1/2$	N_{20}	N_3	4/7	γ_{38}
$-1/2$	$1/2$	N_{20}	N_4	2/7	γ_{39}
$1/2$	$-1/2$	N_{21}	N_3	2/7	γ_{40}
$1/2$	$1/2$	N_{21}	N_4	4/7	γ_{41}
$1/2$	$3/2$	N_{21}	N_5	1/7	γ_{42}
$3/2$	$1/2$	N_{22}	N_4	10/21	γ_{43}
$3/2$	$3/2$	N_{22}	N_5	10/21	γ_{44}
$3/2$	$5/2$	N_{22}	N_6	1/21	γ_{45}
$5/2$	$3/2$	N_{23}	N_5	5/7	γ_{46}
$5/2$	$5/2$	N_{23}	N_6	2/7	γ_{47}
$7/2$	$5/2$	N_{24}	N_6	1	γ_{48}

Table B.4 Rate coefficients for transition between F'=1/2 and F=1/2 in ^{171}Yb. C-G stands for Clebsch-Gordan Coefficient.

m_i	m_f	N_i	N_f	C-G	γ_i
$-1/2$	$-1/2$	N_7	N_1	1/3	γ_7
$-1/2$	$1/2$	N_7	N_2	2/3	γ_8
$1/2$	$-1/2$	N_8	N_1	2/3	γ_9
$1/2$	$1/2$	N_8	N_2	1/3	γ_{10}

Table B.5 Rate coefficients for transition between F'=3/2 and F=1/2 in ^{171}Yb. C-G stands for Clebsch-Gordan Coefficient.

m_i	m_f	N_i	N_f	C-G	γ_i
$-3/2$	$-1/2$	N_3	N_1	1	γ_1
$-1/2$	$-1/2$	N_4	N_1	2/3	γ_2
$-1/2$	$1/2$	N_4	N_2	1/3	γ_3
$1/2$	$-1/2$	N_5	N_1	1/3	γ_4
$1/2$	$1/2$	N_5	N_2	2/3	γ_5
$3/2$	$1/2$	N_6	N_2	1	γ_6

Bibliography

[1] Q. McKnight, A. Dodson, T. Sprenkle, T. Bennett, and S. Bergeson, "Comment on "Laser cooling of ^{173}Yb for isotope separation and precision hyperfine spectroscopy"," Phys. Rev. A **97,** 016501 (2018).

[2] M. Kleinert, M. E. Gold Dahl, and S. Bergeson, "Measurement of the Yb I $^1S_0-^1P_1$ transition frequency at 399 nm using an optical frequency comb," Phys. Rev. A **94,** 052511 (2016).

[3] C. J. Sansonetti, C. E. Simien, J. D. Gillaspy, J. N. Tan, S. M. Brewer, R. C. Brown, S. Wu, and J. V. Porto, "Absolute Transition Frequencies and Quantum Interference in a Frequency Comb Based Measurement of the ^{6,7}Li *D* Lines," Phys. Rev. Lett. **107,** 023001 (2011).

[4] R. C. Brown, S. Wu, J. V. Porto, C. J. Sansonetti, C. E. Simien, S. M. Brewer, J. N. Tan, and J. D. Gillaspy, "Quantum interference and light polarization effects in unresolvable atomic lines: Application to a precise measurement of the ^{6,7}Li D_2 lines," Phys. Rev. A **87,** 032504 (2013).

[5] D. R. Paschotta, "Optical Pumping,", 2017.

Index